Korea-Australia Rheology Journal
Vol. 20, No. 3, September 2008 pp. 143-152

Concentration distributions during flow of confined flowing polymer solutions at finite concentration: slit and grooved channel

Juan P. Hernandez-Ortiz[1,2], Hongbo Ma[1], Juan J. de Pablo[1] and Michael D. Graham[1,*]
[1]*Department of Chemical and Biological Engineering, University of Wisconsin-Madison, Madison, WI 53706-1691*
[2]*Departamento de Materiales, Universidad Nacional de Colombia, Sede Medellin, Kra 80 # 65-223, Bloque M3-050, Medellin Colombia*

(Received April 22, 2008)

Abstract

Simulations of solutions of flexible polymer molecules during flow in simple or complex confined geometries are performed. Concentrations from ultradilute up to near the overlap concentration are considered. As concentration increases, the hydrodynamic migration effects observed in dilute solution unidirectional flows (Couette flow, Poiseuille flow) become less prominent, virtually vanishing as the overlap concentration is approached. In a grooved channel geometry, the groove is almost completely depleted of polymer chains at high Weissenberg number in the dilute limit, but at finite concentration this depletion effect is dramatically reduced. Only upon inclusion of hydrodynamic interactions can these phenomena be properly captured.

Keywords : microfluidics, polymer migration, Brownian dynamics, hydrodynamic interactions

1. Introduction

The dynamics of polymer solutions driven by flow in a confined geometry is a fundamental research topic underlying many practical applications, including enhanced oil recovery from porous media and separation of synthetic or biological molecules using various chromatography methods (Agarwal *et al.*, 1994). With recent advances in design and fabrication of novel microfluidic devices for gene mapping (Chan *et al.*, 2004; Jing *et al.*, 1998; Kan *et al.*, 2004), DNA separation and hybridization (Roper *et al.*, 2005; Han and Craighead, 2000; Storm *et al.*, 2005; Streek *et al.*, 2005), this long-standing research topic has attracted renewed interest. In some approaches to this set of problems, simple devices such as channels with rectangular cross-section are used. Other studies, however, have begun to examine the behavior of chains in more complex geometries (Chan *et al.*, 2004; Han and Craighead, 2000; Streek *et al.*, 2005).

Previous studies have shown that during flow in a smooth-walled channel, flexible polymer molecules in solution will migrate towards the channel center, due to the hydrodynamic interactions of the chain segments and the channel walls (Jendrejack *et al.*, 2003a; 2004; Ma and Graham, 2005; Hernandez-Ortiz *et al.*, 2006a). This migration phenomenon has obvious implications for surface-adsorption based chemical and biological applications (Jing *et al.*, 1998; Dimalanta *et al.*, 2004), as molecules that tend to migrate away from the walls are unlikely to adsorb on them. How this phenomenon is affected either by polymer concentration or by introduction of a more complex geometry is as yet unknown. We address both these issues here. Using direct simulations, we investigate the cross-streamline migration of chains in dilute solution during flow in a simple or structured channel, as shown in Fig. 1. A bead-spring chain model for a flexible chain will be used, along with a recently developed method (Hernandez-Ortiz *et al.*, 2007) for efficient simulation of hydrodynamic interactions between polymer segments in a complex geometry.

*Corresponding author: graham@engr.wisc.edu

2. Numerical method

2.1. Polymer model and simulation approach

As is commonly done, we model a linear polymer molecule dissolved in a viscous solvent by a freely jointed bead-spring chain, *i.e.*, N_b beads connected through $N_s = N_b - 1$ springs. Neglecting inertia, the force balance on each bead requires

$$\mathbf{f}_\nu^h + \mathbf{f}_\nu^s + \mathbf{f}_\nu^w + \mathbf{f}_\nu^{bw} + \mathbf{f}_\nu^b = 0, \text{ for } \nu = 1,...,N_b, \quad (1)$$

where, for bead ν, $\mathbf{f}_\nu^h$ is the hydrodynamic force, $\mathbf{f}_\nu^w$ is the bead-to-bead excluded volume force, $\mathbf{f}_\nu^{bw}$ the bead-wall excluded volume force, $\mathbf{f}_\nu^b$ is the Brownian force and $\mathbf{f}_\nu^s$ is the spring force. The characteristic variables are the bead hydrodynamic radius, a, for distance, the bead diffusion

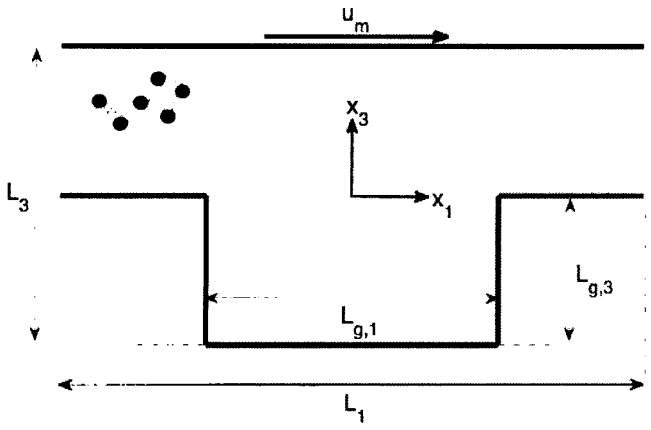

Fig. 1. Schematic of a grooved channel. Shown in the figure is the x_1-x_3 plane cross-section; x_1 is horizontal and x_3 vertical. The simulation domain is periodic in the x_1 and x_2 directions.

time: $\zeta a^2/k_BT$ for time and k_BT/a for force, where k_B is Boltzmann's constant, T the absolute temperature, and ζ the bead friction coefficient, which is related to the solvent viscosity, η, and a through Stokes' law, *i.e.* $\zeta=6\pi\eta a$ (Landau and Lifshitz, 1987; Pozrikidis, 1992). For the spring force, a finitely extensible nonlinear elastic (FENE) spring defined by the following dimensionless potential energy (Bird *et al.*, 1987)

$$\phi^s_{\nu\mu}=\frac{1}{2}b\ln\left(1-\frac{r^2_{\nu\mu}}{b}\right) \tag{2}$$

is used. Here $r_{\nu\mu}=|\mathbf{x}_\nu-\mathbf{x}_\mu|$ is the distance between beads ν and μ and b is the extensibility parameter: $H_s q_0^2/k_BT$, where H_s is the spring constant per spring, $H=H_s/N_s$ is the total spring constant for the molecule and $q_0=L/N_s$ the maximum stretch of each spring. bead-bead and bead-wall excluded volumes are enforced with a repulsive Lennard-Jones potential, where the Euclidean distance is replaced by the wall normal direction for bead-wall interactions. A hydrodynamic interaction parameter (Bird *et al.*, 1987; Ma and Graham, 2005; Hernandez-Ortiz *et al.*, 2006a),

$$h^*=\frac{\zeta}{\eta}\sqrt{\frac{H_s}{36\pi^3 k_BT}} \tag{3}$$

characterizes the ratio between the hydrodynamic and static sizes of each bead of the chain.

The polymer selected for the results presented in this paper is close in size to 1/2 of a λ-phage DNA molecule; $N_s=5$, $b_k=0.106$ μm, $L=10.6$ μm and $h^*=0.25$. With these parameters, the chain radius of gyration $R_g=0.707(k_BT/H)=0.43$ μm, the maximum stretch of each spring $q_0=3.464(k_BT/H)^{1/2}=2.12$ μm and the extensibility parameter $b=60$. The concentration is measured in terms of an effective volume fraction defined by

$$\phi_e=\frac{4}{3}\pi R_g^3\frac{N_c}{V}, \tag{4}$$

where N_c is the number of chains and V is the total fluid volume.

The strength of the flow field is characterized by the Weissenberg number, *Wi*, representing the ratio between the time scale of molecular relaxation to that of solvent deformation. For shear flows is defined by $Wi=\lambda\gamma$, where λ is the longest relaxation time of the molecule and γ a characteristic shear rate. For all cases considered here, γ is the nominal shear rate at the top wall. Due to the fact that in this work we need only an estimate of the longest relaxation time we used the relaxation time from Rouse theory (Hookean springs, free-draining, theta solvent) (Bird *et al.*, 1987)

$$\lambda=\frac{\zeta}{2H}\frac{1}{4sin^2(\pi/2N_b)}. \tag{5}$$

The force balance described above can be written as a system of stochastic differential equations of motion for the bead positions (Öttinger, 1996; Risken, 1989; Gardiner, 1985):

$$d\mathbf{R}=\left[\mathbf{U}_0+\mathbf{D}\cdot\mathbf{F}+\frac{\partial}{\partial\mathbf{R}}\cdot\mathbf{D}\right]dt+\sqrt{2}\mathbf{B}\cdot d\mathbf{W}, \tag{6}$$

where $\mathbf{R}$ is a vector containing the $3N_b$ coordinates of the beads that constitute the polymer chain, with $\mathbf{x}_\nu$ denoting the Cartesian coordinates of bead ν. The vector $\mathbf{U}_0$ of length $3N_b$ represents the unperturbed velocity field, *i.e.* the velocity field in the absence of any polymer molecule. The vector $\mathbf{F}$ has length $3N_b$, with $\mathbf{f}_\nu$ denoting the total non-Brownian, non-hydrodynamic force acting on bead ν. Finally, the $3N_b$ independent components of $d\mathbf{W}$ are obtained from a real-valued Gaussian distribution with mean zero and variance dt (Bird *et al.*, 1987; Öttinger, 1996).

The motion of a bead of the chain perturbs the entire flow field, which in turns affects the motion of the other beads. These hydrodynamic interactions (HI) enter the polymer chain dynamics through the 3×3 block components ($\mathbf{D}_{\nu\mu}$) of the $3N_b\times3N_b$ diffusion tensor, $\mathbf{D}=k_BT\mathbf{M}$ ($\mathbf{M}$ is the mobility tensor), which may be separated into the bead Stokes drag and the hydrodynamic interaction tensor, $\boldsymbol{\Omega}_{\nu\mu}$ (Bird *et al.*, 1987; Öttinger, 1996);

$$\mathbf{D}_{\nu\mu}=[\delta\delta_{\nu\mu}+\boldsymbol{\Omega}_{\nu\mu}], \tag{7}$$

where δ is a 3×3 identity matrix and $\delta_{\nu\mu}$ is the Kronecker delta. Computation of $\boldsymbol{\Omega}\cdot\mathbf{f}$ will be discussed below. The Brownian perturbation is coupled to the hydrodynamic interactions through the fluctuation-dissipation theorem (Öttinger, 2005; Reichl, 1998; Zwanzig, 2001)

$$\mathbf{D}=\mathbf{B}\cdot\mathbf{B}^{\mathrm{T}}. \tag{8}$$

2.2. Computation of hydrodynamic interactions

While the equilibrium structure and properties of confined polymeric solutions are fully determined by the polymer-wall and inter-particle interaction energy functions, the dynamics is significantly affected by hydrodynamic forces. Hydrodynamic interactions (HI) must be included in order to capture experimentally observed phenomena related to transport (*e.g.* diffusion coefficients, migration, *etc.*) (Jendrejack *et al.*, 2004; Ma and Graham, 2005). A common way to include HI is to assume that each bead is a point force; the velocity perturbation is then obtained as a sum of fundamental singular solutions of Stokes' equations.

Consider Stokes equations for a flow driven by a distribution of N point forces,

$$\begin{aligned} -\nabla p+\eta\nabla^2\mathbf{u}(\mathbf{x}) &= -\rho(\mathbf{x}) \\ \nabla\cdot\mathbf{u}(\mathbf{x}) &= 0 \end{aligned}, \tag{9}$$

where the force density is $\rho(\mathbf{x})=\sum_{v=1}^{N}\mathbf{f}_v\delta(\mathbf{x}-\mathbf{x}_v)$. Here $\mathbf{f}_v$ is the force exerted on the fluid at point $\mathbf{x}_v$. For an unbounded domain the resulting velocity field is $\mathbf{u}(\mathbf{x})=\sum_v\mathbf{G}(\mathbf{x}-\mathbf{x}_v)\cdot\mathbf{f}_v$, where $\mathbf{G}(\mathbf{x})$ is the free-space Green's function or fundamental solution of the Stokes equations, known as the Stokeslet, given by (Pozrikidis, 1992; Batchelor, 1967; Power and Wrobel, 1995)

$$\mathbf{G}(\mathbf{x})=\frac{1}{8\pi\eta r}\left[\delta+\frac{\mathbf{xx}}{r}\right], \tag{10}$$

where $r=|\mathbf{x}|$.

Due to the linearity of Stokes equations, the velocity $\mathbf{u}(\mathbf{x}_v)$ of the point force located at $\mathbf{x}_v$, can be expressed as

$$\mathbf{U}=\mathbf{M}\cdot\mathbf{F} \tag{11}$$

where the $3N$ vectors $\mathbf{U}=(\mathbf{u}(\mathbf{x}_1),...,\mathbf{u}(\mathbf{x}_N))$ and $\mathbf{F}=(\mathbf{f}_1,...,\mathbf{f}_N)$ contain the velocities and forces of the point forces and $\mathbf{M}$ is the symmetric $3N\times3N$ mobility matrix (Pozrikidis, 1992; Batchelor, 1967; Power and Wrobel, 1995). The $3N\times3N$ components of the mobility matrix are defined by

$$\mathbf{M}_{v\mu}=\delta_{v\mu}\frac{\delta}{\zeta}+(1-\delta_{v\mu})\mathbf{G}(\mathbf{x}_v-\mathbf{x}_\mu), \tag{12}$$

where $\delta_{v\mu}$ is the Kronecker delta and δ the 3×3 identity matrix. According to Eq. (11) and the self-adjointness of Stokes equations, it is required that $\mathbf{M}=\mathbf{M}^T$.

In conventional Green's function-based methods, $\mathbf{M}$ is computed explicitly; the resulting matrix-vector operation to determine $\mathbf{U}$ requires $O(N^2)$ operations. Additionally, for non-periodic domains appropriate boundary conditions must be included in order to correctly calculate the velocity; for example $\mathbf{u}(\mathbf{x})=0$ for no-slip boundaries. For example, Jendrejack *et al.* (2003a; 2003b; 2004) enforced the boundary conditions with solutions using finite element methods; the quadratic scaling limits analysis to small systems. Hernandez-Ortiz *et al.* (2006b) generalized a method developed by Mucha *et al.* (2004); the method scales as $O(N^{1.66})$ but is restricted to slit geometries. There are some methods that allow the calculation of $\mathbf{U}=\mathbf{M}\cdot\mathbf{F}$ by $O(N\log N)$ calculations in periodic domains. For periodic domains, there are Ewald sum and particle-mesh Ewald (PME) methods that are based on the Hasimoto (1959) solution for Stokes flow driven by a periodic array of point forces.

In the present work, $\mathbf{U}=\mathbf{M}\cdot\mathbf{F}$ is determined implicitly, for any geometry (with appropriate boundary conditions), through a newly developed generalization of particle-mesh Ewald methods that we denote the General Geometry Ewald-like Method (GGEM) (Hernandez-Ortiz *et al.*, 2007). GGEM starts with the restatement of the force-density expression in Eq. (9):

$$\rho(\mathbf{x})=\rho_l(\mathbf{x})+\rho_g(\mathbf{x}), \tag{13}$$

similar to conventional PME methods (Hockney and Eastwood, 1988; Deserno and Holms, 1998). Here the "local" density is defined by

$$\rho_l(\mathbf{x})=\sum_{v=1}^{N}\mathbf{f}_v[\delta(\mathbf{x}-\mathbf{x}_v)-g(\mathbf{x}-\mathbf{x}_v)], \tag{14}$$

which drives the local contribution of the velocity field, $\mathbf{u}_l(\mathbf{x})$; and, the "global" density is

$$\rho_g(\mathbf{x})=\sum_{v=1}^{N}\mathbf{f}_v[g(\mathbf{x}-\mathbf{x}_v)], \tag{15}$$

responsible for the global contribution of the velocity field, $\mathbf{u}(\mathbf{x})$. By linearity $\mathbf{u}(\mathbf{x})=\mathbf{u}_l(\mathbf{x})+\mathbf{u}_g(\mathbf{x})$. The screening function, $g(\mathbf{x})$, satisfies

$$\int_{all\ space} g(\mathbf{x})d\mathbf{x}=1. \tag{16}$$

The local velocity, $\mathbf{u}_l(\mathbf{x})$, is calculated assuming an unbounded domain: $\mathbf{u}_l(\mathbf{x})=\sum_v^N\mathbf{G}_l(\mathbf{x}-\mathbf{x}_v)\cdot\mathbf{f}_v$, where $\mathbf{G}_l(\mathbf{x})$ is composed of a free-space Stokeslet minus a smoothed Stokeslet obtained from the solution of Stokes equations with the forcing term given by the function $\rho_g(\mathbf{x})$. For the Stokes equations we found that a modified Gaussian force density defined by

$$g(r)=\left(\frac{\alpha^3}{\pi^{3/2}}\right)e^{(-\alpha^2r^2)}\left[\frac{5}{2}-\alpha^2r^2\right], \tag{17}$$

yields a simple expression for $\mathbf{G}_l(\mathbf{x})$:

$$\mathbf{G}_l(\mathbf{x})=\frac{1}{8\pi\eta}\left[\delta+\frac{\mathbf{xx}}{r^2}\right]\frac{\mathrm{erfc}(\alpha r)}{r}-\frac{1}{8\pi\eta}\left[\delta-\frac{\mathbf{xx}}{r^2}\right]\frac{2\alpha}{\pi^{1/2}}e^{(-\alpha^2r^2)}. \tag{18}$$

Because $\mathbf{G}_l(\mathbf{x})$ decays exponentially on the length scale α^{-1}, in practice the local velocity can be computed, as in normal Ewald methods, by only considering near-neighbors to each particle v (Hockney and Eastwood, 1988).

The global velocity is due to the force distribution $\rho_g(\mathbf{x})$.

In Ewald formulations this solution is given in Fourier space. For a general domain, on the other hand, one can find the solution to Stokes' equation numerically, requiring that $\mathbf{u}_l(\mathbf{x})+\mathbf{u}_g(\mathbf{x})$ satisfy appropriate boundary conditions. At a no-slip boundary we would require $\mathbf{u}_g(\mathbf{x})=-\mathbf{u}_l(\mathbf{x})$. For problems with periodic boundary conditions, Fourier techniques can be used to guarantee the periodicity of the global velocity $\mathbf{u}_g$. The periodicity on the local velocity, $\mathbf{u}_l$, is obtained using the minimum image convention. The solution is obtained on a set of M discrete points on a mesh; in this regard, GGEM resembles a PME method where the assignment function is replaced by the delta function (Hockney and Eastwood, 1988; Deserno and Holms, 1998). In a general domain, many techniques (finite differences, finite elements, spectral methods) can be used to find the global contribution; after the mesh is resolved, interpolation can be used to get the value of the global velocity at the location $\mathbf{x}_v$ of each point. Specifics of the spatial discretizations are presented with the results.

For many applications, the point-particle approximation is not desired; in particular, as the concentration of particles increases, the probability that particles will overlap, having unphysical velocities, increases. To avoid this problem, the particle hydrodynamic radius, a, can be used to define a new smoothed-force density which will give a non-singular velocity. This is achieved by replacing the Stokeslet by a regularized Stokeslet, using the modified Gaussian force density of Eq. (17), with α replaced by ξ, where $\xi\sim a^{-1}$. In this case, $\mathbf{G}_l(\mathbf{x})$ is replaced by

$$\mathbf{G}_l^R(\mathbf{x})=\frac{1}{8\pi\eta}\left[\delta+\frac{\mathbf{xx}}{r^2}\right]\left[\frac{\mathrm{erf}(\xi r)}{r}-\frac{\mathrm{erf}(\alpha r)}{r}\right]+$$

$$\frac{1}{8\pi\eta}\left[\delta-\frac{\mathbf{xx}}{r^2}\right]\left[\frac{2\alpha}{\pi^{1/2}}e^{(-\xi^2r^2)}-\frac{2\alpha}{\pi^{1/2}}e^{(-\alpha^2r^2)}\right], \qquad (19)$$

where the superscript R stands for regularized force density. For $\xi^{-1}=3a/\sqrt{\pi}$, the maximum fluid velocity is equal to that of a particle with radius a and the pair mobility remains positive-definite. For the regularized version of GGEM, $\mathbf{M}=\mathbf{M}^{\mathrm{T}}$ if the boundary condition on $\mathbf{u}_g$ remains the same as for the point force version, at the cost of a violation of the no-slip boundary condition for points within $\sim\xi^{-1}$ from the wall (which would normally be prevented by an excluded volume interaction).

Because GGEM yields $\mathbf{M}\cdot\mathbf{F}$ without explicit construction of $\mathbf{M}$, it is desired to be able to time-integrate Eq. (6) without requiring this product, *i.e.*, a "matrix-free" formulation. Fixman (1978) (see also Grassia *et al.*, 1995) proposed a method to time-integrate this system without needing to evaluate $\partial/\partial\mathbf{R}\cdot\mathbf{D}$:

$$\mathbf{R}^*=\mathbf{R}(t)+[\mathbf{U}_0(\mathbf{R})+\mathbf{M}(\mathbf{R})\cdot\mathbf{F}(\mathbf{R})]\Delta t+\sqrt{2}\mathbf{D}(\mathbf{R})\mathbf{B}^{-1}(\mathbf{R})\cdot\Delta\mathbf{W}(t)$$

$$\mathbf{R}(t+\Delta t)=\mathbf{R}(t)+[\mathbf{U}_0(\mathbf{R}^*)+\mathbf{M}(\mathbf{R}^*)\cdot\mathbf{F}(\mathbf{R}^*)]\Delta t+\sqrt{2}\mathbf{D}(\mathbf{R}^*)\mathbf{B}^{-1}(\mathbf{R})\cdot\Delta\mathbf{W}(t) \qquad (20)$$

Now it only remains to evaluate $\mathbf{B}^{-1}\cdot d\mathbf{W}$ in a matrix-free way. As also noted by Fixman (1986), this can be done by a Chebyshev polynomial approximation method that requires only matrix-vector products, not the matrix itself. This approach has already been implemented in unbounded or periodic domains (Jendrejack *et al.*, 2000; 2002; Branchio and Brady, 2003; Stoltz *et al.*, 2006) as well as simple bounded domains (Jendrejack *et al.*, 2003a; 2003b; 2004; Hernandez-Ortiz *et al.*, 2006a; 2006b); with GGEM it can be directly generalized to arbitrary domains. Here, GGEM will keep the $O(N)$ scaling by relying on a good guess for the iterative process in the global calculation; the solution given by the free draining diffusion tensor times the force vector serves this purpose for each term in the polynomial approximation.

3. Results

3.1. Plane Couette and Poiseuille geometries

We now examine the effect of concentration on migration in a plane Couette and Poiseuille flow geometries. We fix the channel height B at $10(k_BT/H)^{1/2}$ and the dimension P in the periodic directions (x_1 and x_2) at $30(k_BT/H)^{1/2}$. For these computations, the global contribution to the hydrodynamic interactions is calculated on a lattice-like mesh using fast Fourier transforms (FFT) in the two periodic directions and a second order finite difference (FDM) scheme for the confined direction (x_3). The FFT is imple-

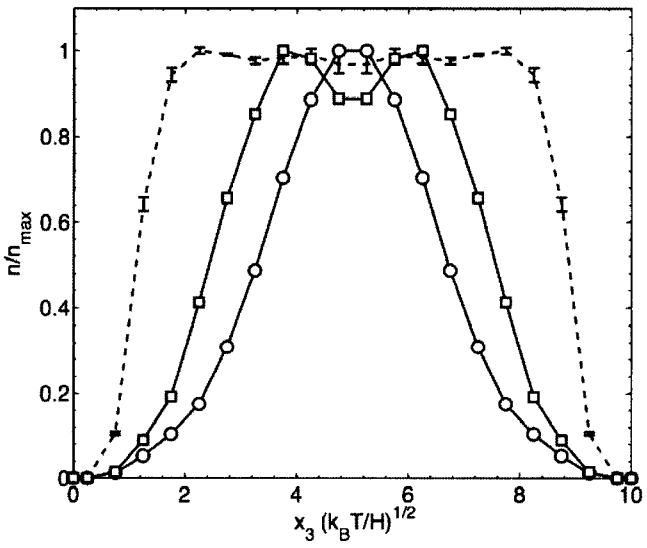

Fig. 2. Steady-state center-of-mass density profiles for an ultradilute concentration ($\phi_e=5.0\cdot10^{-4}$) at equilibrium and at $Wi=20$ for Couette and pressure-driven flow. Walls are located at $x_3=0$ and $x_3=10(k_BT/H)^{1/2}$. This profile is taken after 20 chain diffusion times over the wall separation. Hydrodynamic interactions are included.

mented through the FFTW library (Frigo and Johnson, 1997; 2005), while the FDM is solved with a regular LU decomposition routine (Press *et al.*, 1992).

As a starting point, we show in Fig. 2 the predicted concentration profiles at infinite dilution as a function of cross-sectional position at equilibrium ($Wi=0$) and at $Wi=20$. A substantial hydrodynamic depletion layer is apparent for both Couette and Poiseuille flow at this Weissenberg number; additionally a dip in concentration occurs near the centerline in the Poiseuille flow case; as shown by Jendrejack *et al.* (2004) and Ma and Graham (2005), this arises due to the variation of chain diffusivity displayed by chains exposed to different local strain rates. In the absence of hydrodynamic interactions (HI), the concentration profile would remain virtually unchanged from equilibrium -- the only change in that case is due to the change in chain-wall steric interactions due to the flow-induced change in chain conformations.

As concentration increases, significant changes in the concentration profiles occur. Fig. 3 shows the concentration profiles in Couette and Poiseuille flow at $Wi=20$, at (nominal) concentrations ranging from $4.7\cdot10^{-3}$ to 0.19. The hydrodynamic depletion layer begins to be substantially reduced once $\phi_e \geq 0.01$, and once $\phi_e \geq 0.1$ the concentration profiles closely resemble that at equilibrium. One possible explanation for this change is the screening of chain-wall hydrodynamic interactions that arises for semidilute solutions, but the concentrations here are below

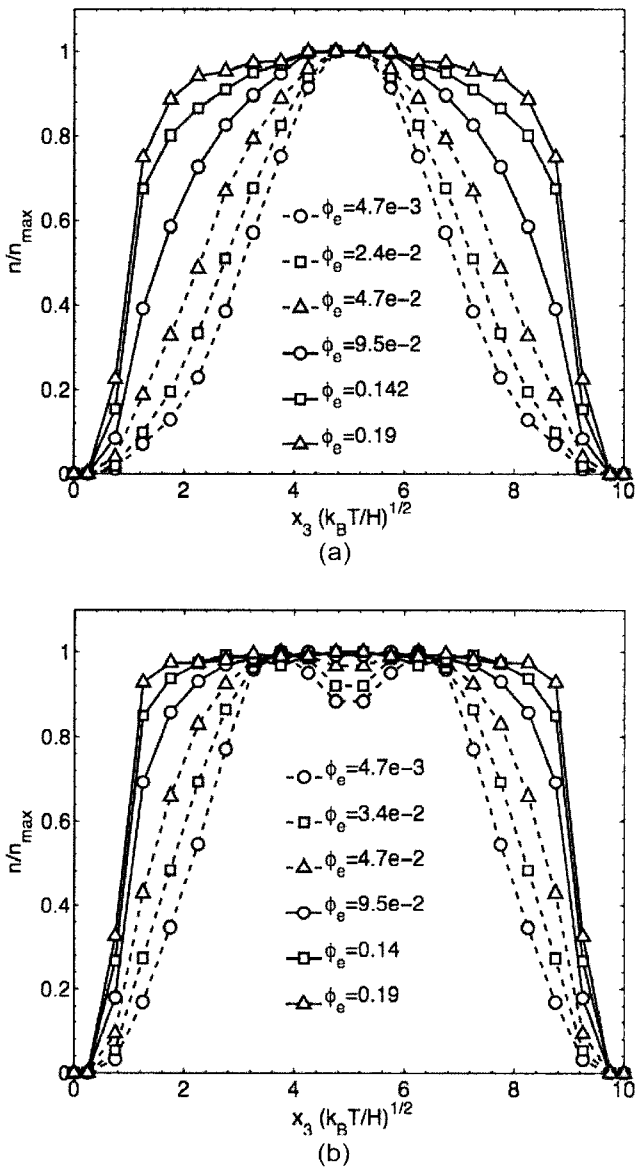

Fig. 3. Steady-state center-of-mass density profiles for different concentrations at $Wi=20$ for (a) Couette and (b) pressure-driven flow. Walls are located at $x_3=0$ and $x_3=10(k_BT/H)^{1/2}$. Hydrodynamic interactions are included.

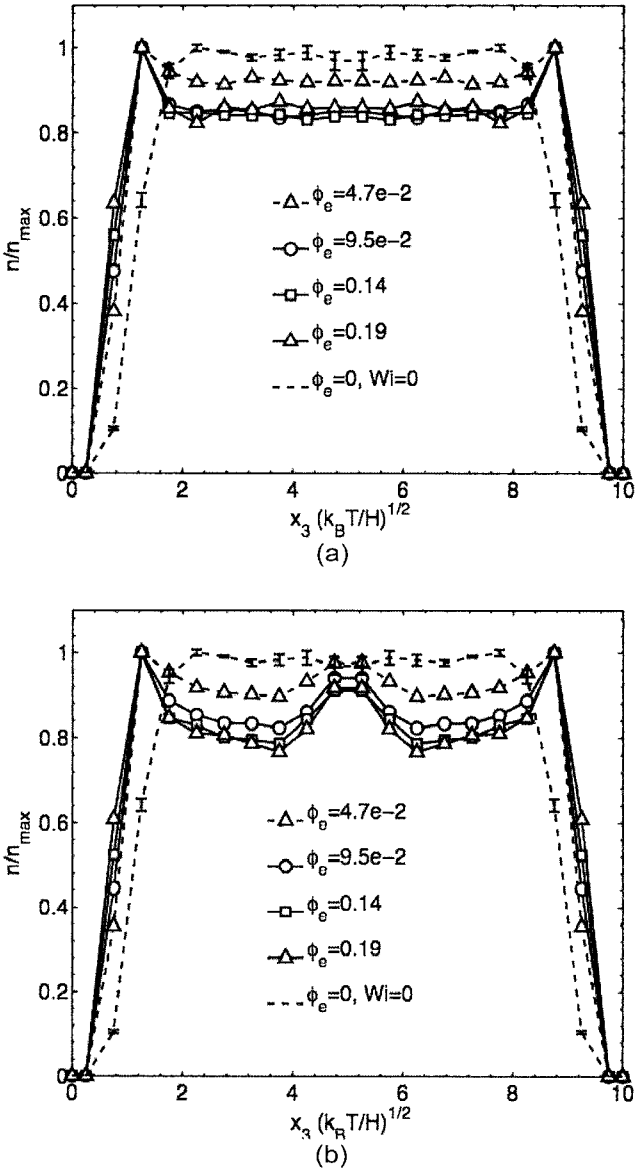

Fig. 4. Steady-state center-of-mass density profiles for different concentrations at $Wi=20$ for (a) Couette and (b) pressure-driven flow. Walls are located at $x_3=0$ and $x_3=10(k_BT/H)^{1/2}$. These are free-draining (FD) chains - hydrodynamic interactions are not included.

the semidilute crossover so screening may not provide a full explanation. Indeed we will see below in the grooved channel results that hydrodynamic interactions are clearly continuing to play a role at the highest concentrations considered here. Indeed, the importance of including hydrodynamic interactions can be seen by comparing with "free-draining" (FD) simulations where they are not included, shown in Fig. 4. The results that neglect hydrodynamic interactions are clearly qualitatively incorrect.

At finite concentration the variation in polymer concentration affects the local viscosity and thus the velocity profile. Velocity profiles as a function of concentration are shown in Fig. 5 under the same conditions considered above. For these simulations, the wall shear stress is constant for all cases, and since the polymer concentration at the wall is zero (because the polymer concentration there is zero), the wall shear rate is also the same for all simulations shown here. The velocity profiles change significantly with concentration; the Couette flow profiles in particular clearly show the emergence of an apparent slip phenomenon -- the linear velocity profile away from the walls extrapolates to zero some distance past the walls, showing an extrapolation (slip) length of about $2(k_BT/H)^{1/2}$.

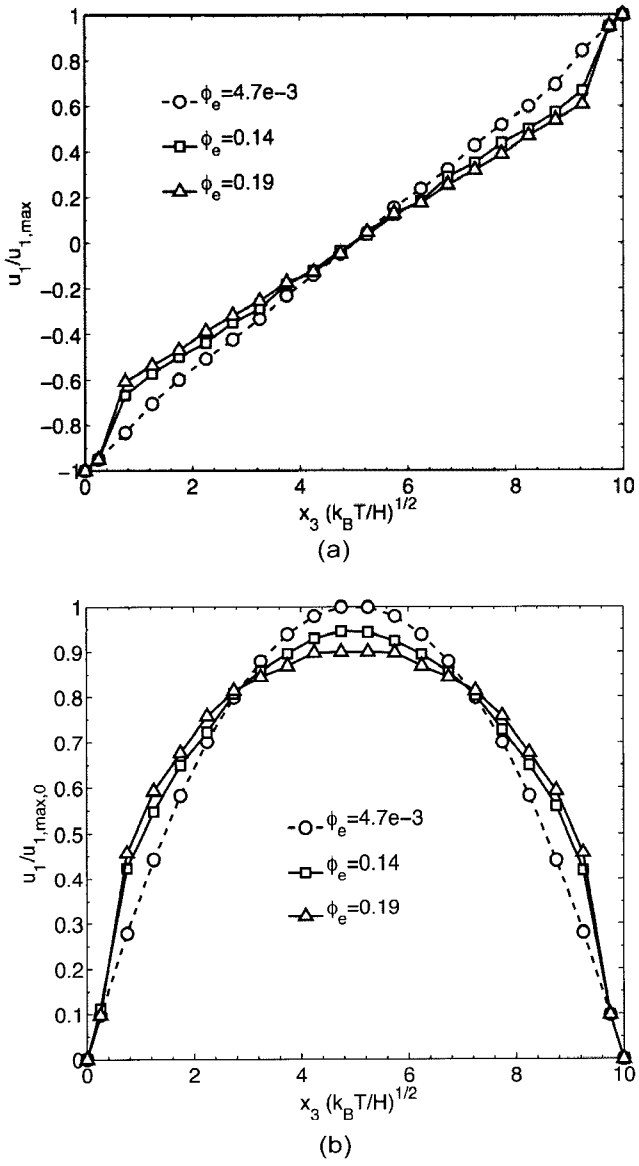

Fig. 5. Mean velocity profile for different concentrations at $Wi=20$: (a) Couette and (b) pressure-driven flow. Hydrodynamic interactions are included.

3.2. Grooved channel

We turn now to the prediction of polymer concentration distributions in flow in a channel with cross-stream-oriented grooves, to understand the effect of concentration and hydrodynamics on the partitioning of polymer chains between the main channel and the groove during flow. One key observation from the above results in a simple geometry is that even up to close to the overlap concentration, the neglect of hydrodynamic interactions in the computation of confined flowing polymer solutions can lead to qualitatively incorrect results. We shall see that a similar conclusion holds here.

Consider a grooved channel as shown in Fig. 1. The bulk channel has height $L_3=20(k_BT/H)^{1/2}$ and length $L_1=40(k_BT/H)^{1/2}$, while the groove has length $L_{g,1}=20(k_BT/H)^{1/2}$ and depth of $L_{g,3}=20(k_BT/H)^{1/2}$. The channel has dimension of $L_2=20(k_BT/H)^{1/2}$ in the neutral x_2-direction. The upper wall is moved in the positive x_1-direction with a speed u_m to shear the fluid in the channel. The strength of the flow field is characterized, similar to the slit channel, by a Weissenberg number using the shear rate $u_m/(L_3-L_{g,3})$.

The global contribution (solution of Stokes equations with the global force density), is solved with a finite element method (FEM) formulation, where linear 8-noded brick elements are used for the velocity and constant elements are used for the corresponding global pressure. The solution of the linear system is done through a fast LU decomposition solver for sparce matrices, SUPER-LU (Demmel *et al.*, 1999). The LU decomposition of the matrix is done at the beginning of the simulation and during the time advancement the only computation required is back-substitution, making the GGEM algorithm very computationally efficient.

Fig. 6(a) shows the geometry under consideration and a contour plot (normalized with the maximum concentration) of the concentration profile at equilibrium in the dilute limit. Aside from the steric depletion layers near the walls, the concentration is uniform. To generate flow in this geometry, the top boundary is moved (so in the absence of the groove we would have Couette flow). Boundary conditions at the left and right boundaries are periodic and the domain is also periodic in the direction perpendicular to the plane of the paper. The Weissenberg number is based on the nominal shear rate that would be present in the absence of the groove. Figs. 6(b) and (c) show the concentration

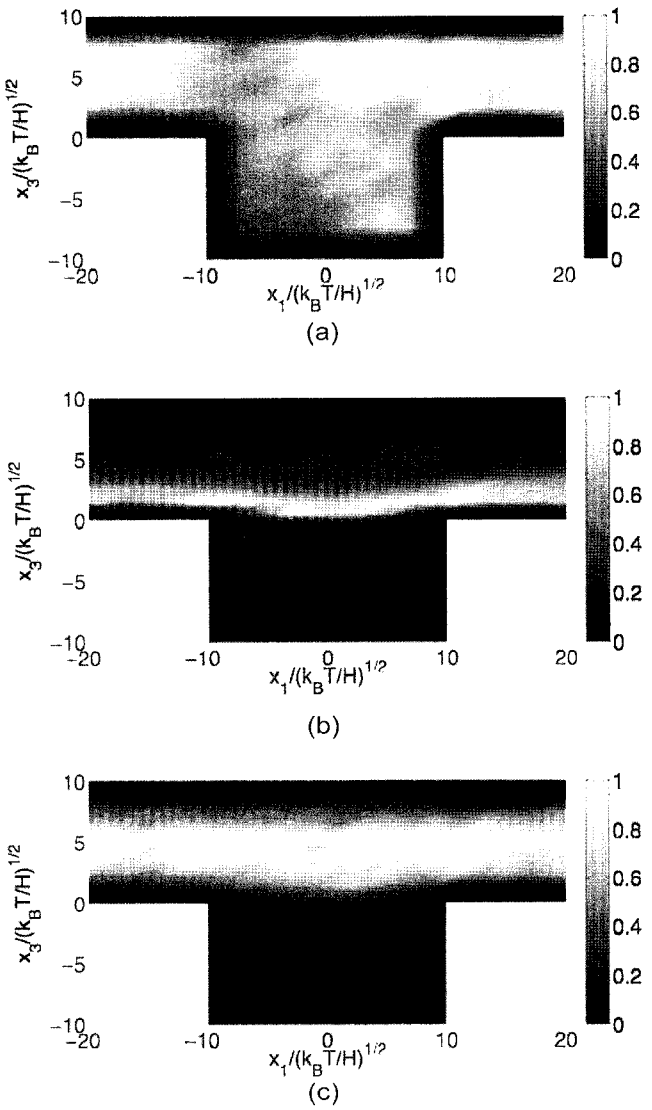

Fig. 6. Steady-state chain center-of-mass distribution, for an infinite dilute concentration ($\phi_e = 1.0 \cdot 10^{-4}$), at equilibrium (a) and in a flowing polymer solution at $Wi = 20$ for FD (b) and HI (c) chains.

profiles at $Wi = 20$ for a very dilute system in the absence (b) and presence (c) of hydrodynamic interactions. One common feature of the two cases is that the groove is almost completely depleted of polymer chains.

We now explain the depletion of polymer chains from the groove. Because of the wall excluded volume effect, a polymer chain center-of-mass cannot move closer to solid walls than the polymer molecule size (roughly its radius of gyration R_g), resulting in a steric depletion layer next to each confining surface. The steric depletion layers are shown as grey regions in Fig. 7. The steric depletion layer above the upstream wall is convected across the top of the groove, which gives rise to a boundary layer of thickness R_g that polymer chains need to diffuse across in order to cross the separatrix streamline (*i.e.* the streamline con-

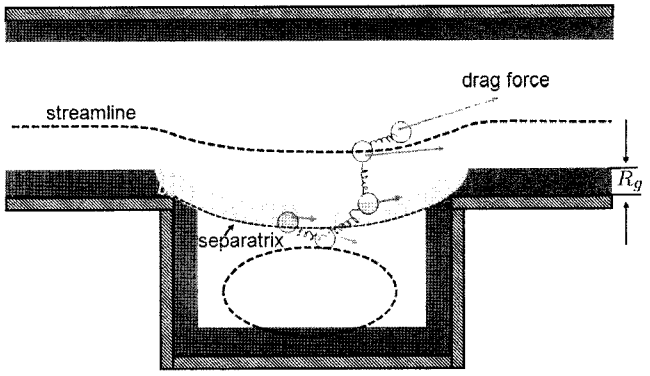

Fig. 7. Schematic of a chain crossing the boundary layer near the separatrix at the top edge of the groove.

necting the two corners of the groove) and enter the groove. In other words, the center of mass of a chain at the upstream edge of the cavity is at least a distance R_g from the separatrix, which it must cross to enter the cavity.

One mechanism for the chain to cross the boundary layer is by diffusion. However, the chain only has limited time, the convective time along the separatrix, to diffuse into the cavity. We define the cavity Peclet number Pe_C as the ratio of the diffusion time of a chain across the boundary layer to its convective time along the separatrix,

$$Pe_C = \frac{R_g^2/D}{L_{g,1}/u_m}, \tag{21}$$

where $D \sim R_g^2/\lambda$ is the diffusivity for the chain. Note that the cavity Peclet number is proportional to Weissenberg number in shear flow; in our simulation it is about 10 at Weissenberg number of 20. In other words, the chain is only in the boundary layer above the groove for 1/10 of the expected time needed for it to diffuse across the boundary layer. The other mechanism for the chain to cross the boundary layer lies in the fact that the flow is stronger outside the groove than inside. Due to the Brownian motion, a few beads of a chain originally inside the groove diffuse out of the groove, as shown in Fig. 7. Since the flow field outside the groove is stronger, the beads outside feel larger drag forces and they will eventually pull the remaining beads out of the groove. On the other hand, if a chain originally outside the groove is to enter, it must rely on the Brownian motion to bring most of its beads into the groove to overcome the stronger drag force outside. Otherwise, the chain will be kept out of the groove. As a result, the chain center-of-mass distribution is lower inside the groove than that outside.

Although both simulations predict the depletion from the grooves, their predictions for the concentration profile in the main channel are rather different. The free draining simulations predicts a band of high concentration on the grooved side of the channel; this arises because chains get "hooked" on the downstream corner of the groove and

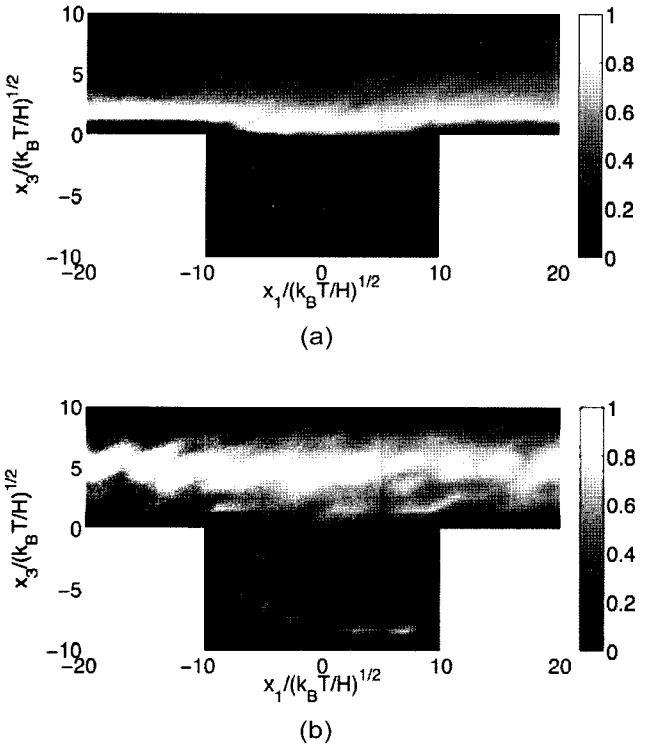

Fig. 8. Steady-state chain center-of-mass distribution, for $\phi_e=0.12$, in a flowing polymer solution at $Wi=20$ for FD (a) and HI (b) simulations.

their vertical motion is thus hindered. In the simulations that include hydrodynamic interactions, however, this phenomenon does not occur because hydrodynamic migration keeps the chains from being close to either the top (smooth) or bottom (grooved) walls -- indeed, for the geometry here the concentration distribution in the main part of the grooved channel is similar to the profile in the absence of the groove.

Turning from the dilute limit to finite concentration, Fig. 8 shows the concentration profiles at $\phi_e=0.12$. Another view of this data is shown in Fig. 9, where we plot normalize concentration vs. vertical position x_3 along the line $x_1=0$ (negative x_3 is in the groove, positive in the main channel). For the free-draining case, the groove is nearly completely depleted of polymers, as in the dilute limit. When hydrodynamic interactions are included, however, the situation changes very significantly. The concentration in the groove is a substantial fraction (about 0.4) of the maximum concentration in the channel. This phenomenon, which is potentially important in applications such as GPC, is not presently understood, but our hypothesis is the following.

As described above for a dilute system, the mechanism by which a chain exits the groove is by diffusion of a sufficient length of it across the separatrix that the flow in the main channel drags the rest of it out. For a chain to re-enter the groove it has to diffuse back across the separatrix -- the

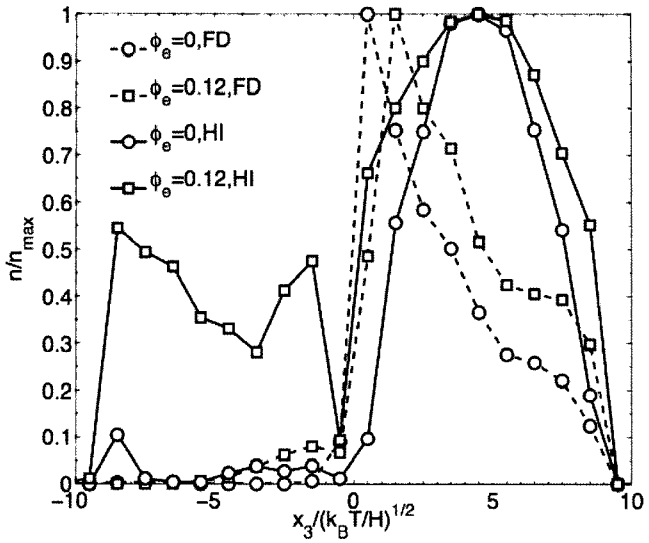

Fig. 9. Vertical cross-section of concentration profiles in the grooved channel along the line $x_1=0$. FD and HI simulation results are shown sat $Wi=20$ for an ultradilute concentration and a finite concentration $\phi_e=0.12$.

flow within the groove is so weak that it is unlikely to assist significantly in dragging the chain back in. In the free-draining simulations, the effect of finite concentration on this mechanism is minor, as shown by the dashed curves on Fig. 9. So how do hydrodynamic interactions change the mechanism at finite concentration? For a chain to leave the groove, it must cross the separatrix to the extent that it can be pulled along by the flow in the main channel. When hydrodynamic interactions are present, the chain that has partially crossed is hydrodynamically coupled to the chains that remain in the groove. The fluid motion generated by pulling one chain tends to pull on the others in the groove; the pulling force is thus distributed across multiple chains and the effective hydrodynamic drag on the pulled chain is higher than it would be in the absence of hydrodynamic interactions. Accordingly, the chain moves more slowly across the separatrix and is less likely to get pulled all the way into the main flow before reaching the downstream corner and convecting down into groove. Thus hydrodynamic interactions decrease the probability that chains will cross the separatrix to leave the groove and thereby increase the steady state concentration of chains within it.

4. Conclusions

Simulations have been performed to predict the effect of concentration on the spatial distribution of polymer molecules during flow in confined geometries. These are the first to systematically include hydrodynamic interactions, and they illustrate that simulations that do not include them yield qualitatively incorrect results. In simple plane Cou-

ette and Poiseuille flow, we see that as concentration increases toward the overlap concentration, the hydrodynamic migration effects found in dilute solution tend to fade away; the concentration distribution is more uniform with increasing concentration. This tendency toward homogenization is also seen in flow over a cross-stream-oriented groove. In dilute solution the groove tends to become depleted of chains due to a combination of transport and steric effects (a prediction that is independent of whether hydrodynamic interactions are included). As overall concentration increases, this depletion effect diminishes dramatically, but only if hydrodynamic interactions are not neglected. We explain this significant concentration-dependence of flow-induced partitioning by noting that the chains in the groove are hydrodynamically coupled, and thus apparently less susceptible to being dragged out of the groove into the main channel.

Acknowledgments

The authors acknowledge financial support from the NSF through the University of Wisconsin Nanoscale Science and Engineering Center, NSF grant DMR-0425880.

References

Agarwal, U. S., A. Dutta, and R. A. Mashelkar, 1994, Migration of macromolecules under flow: the physical origin and engineering implications, *Chem. Eng. Sci.* **49**, 1693.

Banchio, A. J. and J. F. Brady, 2003, Accelerated Stokesian dynamics: Brownian motion, *J. Chem. Phys.* **118**, 10323.

Batchelor, G., 1967, An Introduction to Fluid Dynamics, Cambridge University Press, Cambridge.

Bird, R. B., C. Curtiss, F. R. C. Armstrong, and O. Hassager, 1987, Dynamics of Polymer Liquids: Kinetic Theory, vol. 2, John Wiley & Sons, New York, 2nd Edition.

Chan, E. Y., N. M. Goncalves, R. A. Haeusler, A. J. Hatch, J. W. Larson, A. M. Maletta, G. R. Yantz, E. D. Carstea, M. Fuchs, G. G. Wong, S. R. Gullans and R. Gilmanshin, 2004, DNA mapping using microfluidic stretching and single-molecule detection of fluorescent site-specific tags, *Genome Res.* **14**, 1137.

Demmel, J. W., S. C. Eisenstat, J. R. Gilbert, X. S. Li, and J. W. H. Liu, 1999, A supernodal approach to sparse partial pivoting, *SIAM J. Matrix Analysis and Applications* **20**, 720.

Deserno, M. and C. Holms, 1998, How to mesh up Ewald sums. I. A theoretical and numerical comparison of various particle mesh routines, *J. Chem. Phys.* **109**, 7678.

Dimalanta, E. T., A. Lim, R. Runnheim, C. Lamers, C. Churas, D. K. Forrest, J. J. de Pablo, M. D. Graham, S. N. Coppersmith, S. Goldstein and D. Schwartz, 2004, A microfluidic system for large DNA molecule arrays, *Anal. Chem.* **76**, 5293.

Fixman, M., 1978, Simulation of polymer dynamics. I. general theory, *J. Chem. Phys.* **69**, 1527.

Fixman, M., 1986, Construction of Langevin forces in the simulation of hydrodynamic interaction, *Macromolecules* **19**, 1204.

Frigo, M. and S. G. Johnson, 1997, Tech. Rep. MIT-LCS-TR-728, Massachusetts Institute of Technology, Boston.

Frigo, M. and S. G. Johnson, 2005, The design and implementation of FFTW3, *Proceedings of the IEEE* **93**, 216.

Gardiner, C., 1985, Handbook of Stochastic Methods, Springer, Berlin.

Grassia, P., E. Hinch and L. Nitsche, 1995, Computer simulations of Brownian motion of complex systems, *J. Fluid. Mech.* **282**, 373.

Han J. and H. G. Craighead, 2000, Separation of long DNA molecules in a microfabricated entropic trap array, *Science* **288**, 1026.

Hasimoto H., 1959, On the periodic fundamental solutions of the Stokes equations and their application to viscous flow past a cubic array of spheres, *J. Fluid Mech.* **5**, 317.

Hernandez-Ortiz, J. P., H. Ma, J. J. de Pablo and M. D. Graham, 2006a, Cross stream-line migration on confined flowing polymer solutions: theory and simulation, *Phys. Fluids* **18**, 123101.

Hernandez-Ortiz, J. P., J. J. de Pablo and M. D. Graham, 2006b, $N\log N$ method for hydrodynamic interactions of confined flowing polymer systems: Brownian dynamics, *J. Chem. Phys.* **125**, 164906.

Hernandez-Ortiz, J. P., J. J. de Pablo and M. D. Graham, 2007, Fast computation of many-particle hydrodynamic and electrostatic interactions in a confined geometry, *Phys. Rev. Lett.* **98**, 140602.

Hockney, R. W. and J. W. Eastwood, 1988, Computer Simulation Using Particles, Taylor & Francis, Bristol.

Jendrejack, R. M., M. D. Graham and J. J. de Pablo, 2000, Hydrodynamic interactions in long chain polymers: application of the Chebyshev polynomial approximation in stochastic simulations, *J. Chem. Phys.* **113**, 2894.

Jendrejack, R. M., J. J. de Pablo and M. D. Graham, 2002, Stochastic simulations of DNA in flow: dynamics and the effects of hydrodynamic interactions, *J. Chem. Phys.* **116**, 7752.

Jendrejack, R. M., D. C. Schwartz, M. D. Graham and J. J. de Pablo, 2003a, Effect of confinement on DNA dynamics in microfluidic devices, *J. Chem. Phys.* **119**, 1165.

Jendrejack, R, M., E. T. Dimalanta, D. C. Schwartz, M. D. Graham and J. J. de Pablo, 2003b, DNA dynamics in a microchannel, *Phys. Rev. Lett.* **91**, 038102.

Jendrejack, R. M., D. C. Schwartz, J. J. de Pablo and M. D. Graham, 2004, Shear-induced migration in flowing polymer solutions: simulation of long-chain DNA in microchannels, *J. Chem. Phys.* **120**, 2513.

Jing, J., J. Reed, J. Huang, X. Hu, V. Clarke, J. Edington, D. Housman, T. Anantharaman, E. Huff, B. Mishra, B. Porter, A. Shenker, E. Wolfson, C. Hiort, R. Kantor, C. Aston and D. Schwartz, 1998, Automated high resolution optical mapping using arrayed, fluid-fixed DNA molecules, *Proc. Natl. Acad. Sci. U.S.A.* **95**, 8046.

Kan, C. W., C. P. Fredlake, E. A. S. Doherty and A. E. Barron, 2004, DNA sequencing and genotyping in miniaturized electrophoresis systems, *Electrophoresis* **25**, 3564.

Landau, L. and E. Lifshitz, 1987, Fluid Mechanics, Butterworth-

Heinemann, Oxford, 2nd Edition.

Ma, H. and M. D. Graham, 2005, Theory of shear-induced migration in dilute polymer solutions near solid boundaries, *Phys. Fluids* **17**, 083103.

Mucha, P. Y., S.-Y. Tee, D. A. Weitz, B. I. Shraiman and M. P. Brenner, 2004, A model for velocity fluctuations in sedimentation, *J. Fluid Mech.* **501**, 71.

Öttinger, H. C., 2005, Beyond Equilibrium Thermodynamics, Wiler-Interscience, New York.

Öttinger, H.C., 1996, Stochastic Processes in Polymeric Fluids, Springer, Berlin.

Power H. and L. C. Wrobel, 1995, Boundary Integral Methods in Fluid Mechanics, Computational Mechanics Publications, Southampton.

Pozrikidis, C., 1992, Boundary Integral and Singularity Methods for Linearized Viscous Flow, Cambridge University Press, Cambridge.

Press, W. H., S. A. Teukolsky, W. T. Vetterling and B. P. Flannery, 1992, Numerical Recipes in Fortran 77, Cambridge University Press, Cambridge, 2nd Edition.

Reichl, L., 1998, A Modern Course in Statistical Physics, Wiley-Interscience, New York 2nd Edition.

Risken, H., 1989, The Fokker-Planck Equation, Springer, Berlin, 2nd Edition.

Roper, M. G, C. J. Easley, and J. P. Landers, 2005, Advances in polymerase chain reaction on microfluidic chips, *Anal. Chem.* 77, 3887.

Stoltz, C., J. J. de Pablo and M. D. Graham, 2006, Concentration dependence of shear and extensional rheology of polymer solutions: Brownian dynamics simulations, *J. Rheol.* **50**, 137.

Storm, A. J., J. H. Chen, H. W. Zandbergen and C. Dekker, 2005, Translocation of double-strand DNA through a silicon oxide nanopore, *Phys. Rev. E* **71**, 051903.

Streek, M., F. Schmid, T. T. Duong, D. Anselmetti and A. Ros, 2005, Two-state migration of DNA in a structured microchannel, *Physical Rev. E* **71**, 011905.

Zwanzig, R., 2001, Nonequilibrium Statistical Mechanics, Oxford University Press, Oxford.